ACS MATERIALS LETTERS

www.acsmaterialsletters.org

LETTER

Abundant Active Sites on the Basal Plane and Edges of Layered van der Waals Fe_3GeTe_2 for Highly Efficient Hydrogen Evolution

Amir A. Rezaie,[#] Eunsoo Lee,[#] Diana Luong,[#] Johan A. Yapo, and Boniface P. T. Fokwa*

Cite This: *ACS Materials Lett.* 2021, 3, 313–319

Read Online

ACCESS | Metrics & More | Article Recommendations | Supporting Information

ABSTRACT: van der Waals (vdW) metal chalcogenides have been extensively investigated as electrocatalysts for the hydrogen evolution reaction (HER); however, for the majority of these materials only the edges are active, thereby wasting most of the materials' surfaces. Recent research has focused on finding new materials with active basal planes. Herein, for the first time, we demonstrate that the hexagonal vdW Fe_3GeTe_2 (FGT), also a spintronic candidate material, shows both basal plane and edge site HER activities. Partial exfoliation of bulk FGT through sonication increases both basal plane and edge sites leading to significantly improved overpotential. A subsequent compacting of the sample (using plasma sintering at room temperature) to produce a densified electrode leads to an impressive overpotential to drive a current density of 10 mA/cm^2 of −0.105 V. DFT free energy calculations not only showed that the high activity is due to the abundant active sites present on the hexagonal Te layer in FGT but also presented an even more HER active layer (106) containing both iron and tellurium active sites. Furthermore, the presence of a thin oxide layer on top of the active FGT layers, as found by XPS, suggests that the real active surface is likely a hybrid FGT/oxide layer. These results demonstrate the high basal plane and edge sites HER activity of FGT, thus opening a new avenue for the design and screening of related iron-based vdW materials, their composites, and their surface functionalization as high-performing electrocatalysts.

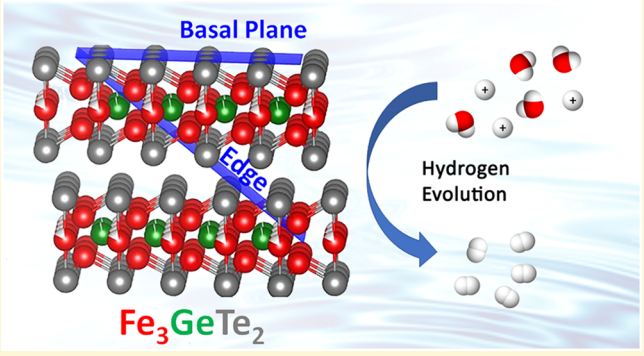

The development of clean and renewable energy is crucial in order to overcome the depletion of fossil fuels while meeting an increase in energy demand.[1,2] Among all the renewable energy sources, hydrogen has been accepted as one of the most promising alternatives to fossil fuels due to its cleanliness, sustainability, and high energy density.[3−5] Through water electrolysis, an environmental-friendly method, hydrogen can be produced to achieve sustainable energy production.[6−8] Currently, platinum-group metals and noble-metal compounds are considered the most efficient hydrogen evolution reaction (HER) electrocatalysts. However, high cost and scarcity of these precious metals impede large-scale utilization and commercialization.[9,10] The development of a highly active and abundant electrocatalyst would overcome these difficulties, providing the necessary breakthrough for a sustainable and clean energy supply.

van der Waals (vdW) layered materials have been known for several decades.[11] However, the interest in these materials has been renewed since the discovery of graphene as the first two-dimensional (2D) material.[12,13] This and various other 2D materials beyond graphene have raised extensive interest in optical, electronic, and energy storage applications.[14−16] Due to intriguing properties, 2D materials are being explored as alternative electrocatalysts.[17−20] Most pristine vdW materials do not show electrochemical activity in their basal planes; thus to improve the activity of the basal plane, various surface modifications such as defect engineering,[21−23] interfacial engineering,[24−26] and doping[27−29] are required. However, if the parent layered material demonstrates activity in the basal plane prior to surface modification, its electrochemical activity can be tremendously improved after further modifications. Consequently, recent research has been focused on the discovery of new basal plane active vdW materials. Among

Received: January 19, 2021
Accepted: February 18, 2021
Published: February 22, 2021

https://dx.doi.org/10.1021/acsmaterialslett.1c00048
ACS Materials Lett. 2021, 3, 313–319

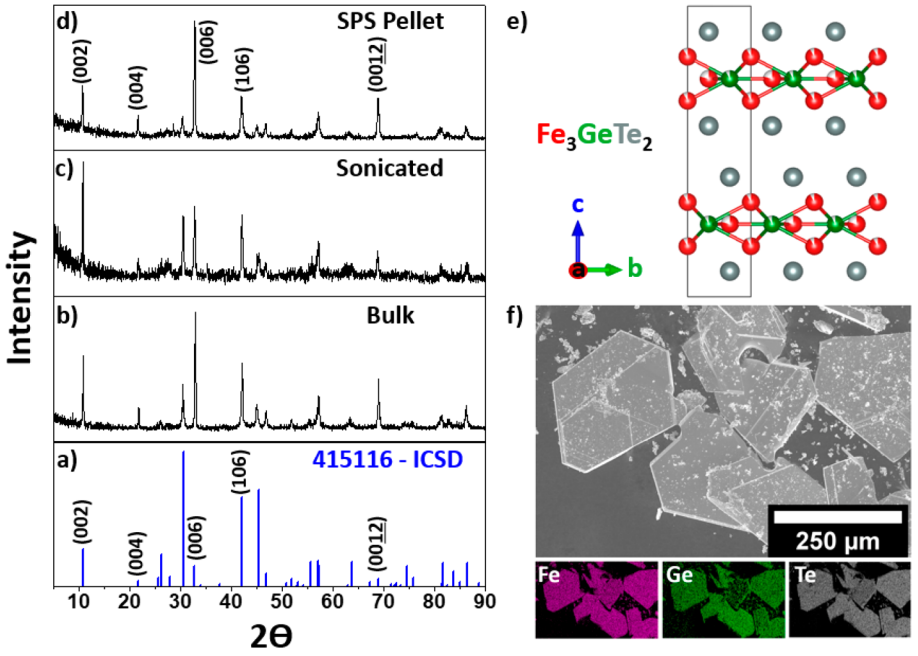

Figure 1. Powder X-ray diffraction patterns of FGT: (a) calculated, (b) bulk, (c) sonicated, and (d) SPS pellet. (e) Crystal structure of FGT and (f) SEM images and EDS mappings of as-synthesized FGT crystals.

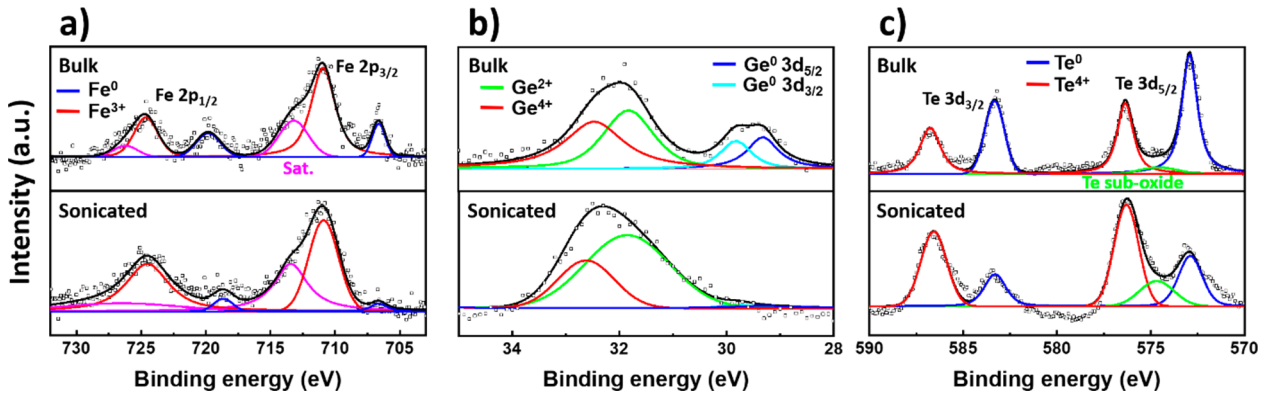

Figure 2. X-ray photoelectron spectroscopy spectra of (a) Fe 2p, (b) Ge 3d, and (c) Te 3d for bulk and sonicated FGT samples. Experimental and fitting data are indicated as (□) and solid lines, respectively.

all the vdW layered materials, Fe_3GeTe_2 (FGT), an itinerant ferromagnet with high stability and high Curie temperature (220 K), has attracted great interest recently in the field of spintronics. FGT has a hexagonal crystal symmetry with space group $P6_3/mmc$, consisting of a "Fe_3Ge" substructure sandwiched between two layers of Te atoms, which are weakly bonded by vdW forces as seen in Figure 1e.[30,31] Very recently, FGT was suggested as a potential electrocatalyst candidate for the oxygen-evolution reaction (OER) and other gas adsorption reactions (CO, NO, etc.).[20,32] However, no theoretical or experimental work has proposed FGT as an active material for HER to the best of our knowledge. Herein, we report on the experimental and theoretical investigations of the HER activity of FGT for the first time. We have investigated FGT's electrochemical activity in three different forms: bulk, partially exfoliated layers (sonicated), and densified layers. We found that FGT is highly active in bulk form already, a finding confirmed by density functional theory (DFT) calculations. Furthermore, the HER activity increases with exfoliation and even more after densification.

The FGT sample was synthesized through a direct solid-state reaction according to previous reports [see the Supporting Information (SI) for more details]. The sample was investigated by powder X-ray diffraction (PXRD) for phase and crystallinity determination, via energy dispersive X-ray spectroscopy (EDS) for elemental analysis and through scanning electron microscopy (SEM) for particle size and morphology determination. According to the PXRD pattern (Figure 1b), all peaks matched those reported for FGT, proving a single-phase synthesis and EDS mapping showed the presence of all three elements as well as their homogeneous distribution (Figure 1f). However, some intensity mismatches were observed in the PXRD pattern for the (*00l*) peaks due to the preferred orientation along the *c*-axis as expected for flat, thin crystals (Figure 1f).

To increase the amount of exposed basal planes, the FGT sample was crushed, and the resulting powder was dispersed in ethanol and ultrasonicated in a vial which was immersed in an ice−water bath for 2 h. Ultrasonication of the FGT powder resulted in smaller particles (Figure S1). PXRD shows an

https://dx.doi.org/10.1021/acsmaterialslett.1c00048
ACS Materials Lett. 2021, 3, 313−319

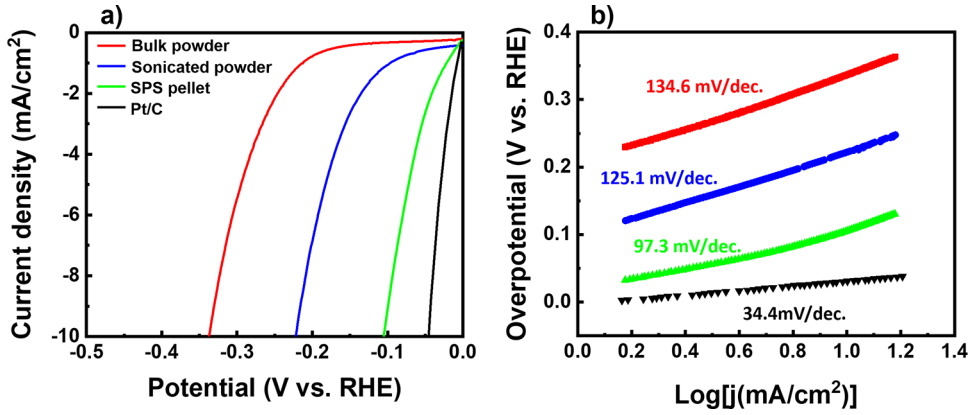

Figure 3. a) Polarization curves of FGT (for various electrode types) and Pt/C. The data were recorded in 1 M KOH at a scan rate of 5 mV/s with iR-correction. b) Tafel plots obtained using the polarization curves in a).

intensity increase for the (002) peak (Figure 1c), indicating abundance of exposed (002) layers and confirming partial exfoliation of the bulk crystals. Interestingly, the (106) peak has become one of the most prevalent intensities, indicating exposure of edges through layer breaking.

The surface chemical composition and the core-level binding energy of the bulk and sonicated FGT were investigated by X-ray photoelectron spectroscopy (XPS). Figure 2 and Table S1 show the oxidation states of the Fe 2p, Ge 3d, and Te 3d species on the analyzed surfaces. As shown in Figure 2a, the high-resolution Fe 2p spectrum is deconvoluted into Fe $2p_{1/2}$ and Fe $2P_{3/2}$: The two peaks at 706.6 eV/719.8 eV originate from the metallic iron (Fe^0 in FGT). The two other doublets at 710.9 and 724.6 eV (with 713.2 and 726.21 eV satellites)[33−36] can be ascribed to Fe^{3+} from the surface oxide layer. The Ge 3d spectrum (Figure 2b) is deconvoluted into Ge $3d_{3/2}$ and Ge $3d_{5/2}$, with the peaks at 29.3/29.8 eV assigned to metallic germanium (Ge^0 in FGT), while those at 31.8 eV (Ge^{2+}) and 32.4 eV (Ge^{4+}) correspond to germanium oxide peaks.[37−39] Finally, the Te 3d spectrum (Figure 2c) is deconvoluted into Te $3d_{3/2}$ and Te $3d_{5/2}$, with the peaks at 572.9/583.3 eV ascribed to metallic tellurium (Te^0 in FGT) and those at 576.4/586.8 eV assigned to Te^{4+}.[40,41] Comparing the non-oxide peaks (Fe^0, Ge^0, and Te^0) to each other in both samples (bulk and sonicated), it is obvious that Te^0 is by far the most abundant on the surface, an indication of a Te-terminated basal plane in FGT, as expected for this Te-terminated vdW atomic structure (Figure 1e). The oxide peaks in all the species reveal that air-exposed surface atoms of FGT have been oxidized. However, this oxide layer is likely very thin because the FGT peaks (Fe^0, Ge^0, and Te^0) are still clearly detectable by XPS. Sonication diminishes the FGT's peak intensities, thereby increasing the amount of surface oxides because more surface area is exposed to oxygen as the particles become smaller. These surface oxides may affect the HER activity of FGT; however, our density functional theory (DFT) calculations show that FGT is already an active HER electrocatalyst on its own (see below). Nevertheless, the effect of the oxides on FGT's HER activity warrants further investigations in the future.

The HER activities of the bulk and sonicated FGT samples were examined in 1 M KOH solution, and their electrodes were prepared via a drop-cast method. The linear sweep voltammetry (LSV) curve of the bulk FGT powder exhibits an overpotential of $\eta_{10} = -0.337$ V at 10 mA/cm^2 (Figure 3a). In comparison, bulk FGT is far better than the most popular layered materials studied as HER catalysts, bulk hexagonal 2H-MoS_2 ($\eta_{10} = -0.83$ V)[42] and 2H-$MoTe_2$ ($\eta_{10} = -0.65$ V),[43] whose active sites are limited solely to the edges. To improve their activity, the basal plane of these materials is usually activated by different surface modifications, which have led to the overpotential improvements given in Table S3, the best value ($\eta_{10} = -0.31$ V) being recorded for the 2H-MoS_2 directly grown on carbon cloth. Interestingly, puckering the chalcogenide layer has proven to be another successful way to activate the basal plane. For example, the basal planes in 3R-MoS_2[42] and 1T′-$MoTe_2$[43] are active showing improved overpotentials of $\eta_{10} = -0.52$ V and $\eta_{10} = -0.34$ V, respectively. FGT has an overpotential comparable to 1T′-$MoTe_2$, hinting at its basal plane activity even though it has an undistorted hexagonal crystal structure with honeycomb Te layers. As demonstrated by PXRD analysis, the bulk FGT sample shows preferred orientation along the *c*-axis [basal plane, (00*l*) reflections], a further indication that the observed activity might be related to the exposed basal plane. Furthermore, XPS analysis shows that Te dominates the surface, a further hint that the Te basal plane is exposed. Indeed, our DFT calculations (see below) show that the flat Te layer in FGT is as active as the puckered Te layer in 1T′-$MoTe_2$.

To confirm and improve this result, we have investigated a sonicated FGT sample, which has more basal planes exposed than the bulk, as shown by PXRD. However, the sonication can also break the layers and provide edge sites which can further impact activity; for example, the PXRD (Figure 1c) shows that the (106) layers are among the most abundant in the sample. Compared to the bulk powder, the sonicated sample shows a significant enhancement (33%) in HER activity with an overpotential of $\eta_{10} = -0.222$ V. To understand this result, we have estimated the available surface-active sites using the electrochemical active surface area (ECSA) method. ECSA was estimated from the electrochemical double-layer capacitance (C_{dl}), with a larger C_{dl} value indicative of more active sites present.[44] Figure S3 shows that the C_{dl} value (22.9 mF/cm^2) of the sonicated powder is larger than that of the bulk powder (16.2 mF/cm^2), confirming that the sonicated sample has more active sites than the bulk. There are two reasons for the increased activity: The exfoliation of the FGT crystals which exposes more basal planes (Figure 1c) and the decrease in particle size (Figure S2) which exposes more edge sites. However, the increased

https://dx.doi.org/10.1021/acsmaterialslett.1c00048
ACS Materials Lett. 2021, 3, 313−319

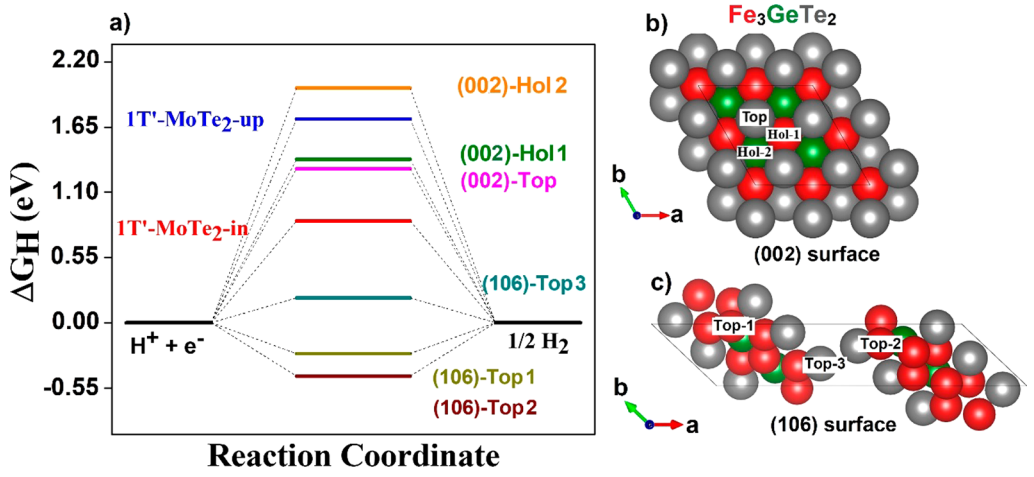

Figure 4. a) The Gibbs free energy (ΔG_H) of H-adsorption on several active sites of FGT and 1T′-$MoTe_2$ from ref 52. b) FGT superstructure models generated for (002) and (106) surfaces with the top and hollow sites indicated.

formation of oxide layers on the surface after sonication could also play a role.

Improving the HER activity of vdW transition metal dichalcogenides (TMDs) is currently one of the most attractive research areas, where defect engineering is being used for activating the inactive basal planes of hexagonal TMDs (Table S3). For monoclinic 1T′-$MoTe_2$, which has an active basal plane, a different strategy was recently employed to boost its HER activity: in fact, its catalytic performance was improved dramatically when the electrode was held at a cathodic bias. As a result, the overpotential required to maintain a current density of 10 mA cm^{-2} improved from −0.320 V to −0.178 V.[45] This is an extraordinary result which showcases the ease with which the HER activity of basal plane active materials can be improved. During our recent studies of another group of basal plane active materials (transition metal diborides), we discovered that their HER activity can be drastically improved by efficiently covering the electrode, thus taking advantage of the basal plane activity.[46−48] We have applied this strategy to further improve the activity of FGT. The sonicated FGT sample was compressed into a pellet through spark plasma sintering (SPS) at room temperature to achieve a densified disk (see the Supporting Information). As shown in Figure S2c, the electrode surface is denser than the other electrodes. This type of electrode exposes more basal planes compared to the drop-cast method; however, the sonication also breaks the layers and provides edge sites which can further impact activity. As shown in Figure S2c, the disk-type electrode provides a homogenous coverage of the FGT particles if compared to the other electrodes (Figures S2a and S2b). The PXRD pattern of the SPS pellet (Figure 1d) shows an intensity increase of the (*00l*) peaks pointing toward a preferred orientation and the presence of more basal planes. Interestingly, this PXRD pattern is almost identical to that recorded for a single crystal of FGT (Figure S4), thus hinting at a nearly single-crystal-like layer arrangement of the FGT particles in the SPS pellet. However, as pointed out above, the (106) peak still remains one of the dominant intensities and thus may have an impact on activity (see below). This condensed, highly oriented (single-crystal-like) electrode dramatically improves all electrochemical parameters of FGT. The obtained overpotential (η_{10} = −0.105 V) not only is more than twice lower than that of the sonicated sample (η_{10} = −0.222 V) but also is the lowest value reported so far for all bulk TMDs electrocatalysts, to the best of our knowledge. Furthermore, the path for the electrodes to transfer electrons from the electrode's substrate (in this work, it is a Cu plate) to the active sites is hugely facilitated by the better electrode coverage of the densified electrode, leading to a more than 2-fold increase in the C_{dl} value (52.7 mF/cm^2) if compared to that of the sonicated sample (22.9 mF/cm^2), thus confirming the overpotential findings. Interlayer electron transfer is the dominant mechanism for HER activity in layered materials,[49] so by reducing the distance between the particles (densification), this makes it easier for electrons to traverse through the layered particles. This is further supported by the EIS data in Figure S8 and Table S4. The charge transfer resistance (R_{ct}) derived from the Nyquist plot can be fitted using an equivalent circuit model consisting of a series resistance (R_s, mainly the solution resistance) and a constant phase element (CPE). The SPS electrode has a much smaller R_{ct} (9.71 Ω) than the sonicated electrode (24.6 Ω), supporting the idea that electrons will move faster in the former and thus boosting its charge transfer rate during HER.

The Tafel slope is an inherent catalyst property regulated by the rate-determining step of HER, with a small slope being desirable to drive a large catalytic current density at low overpotential. From the Tafel plots (Figure 3b), the bulk powder and the sonicated powder display a slope of 134.6 mV/dec and 125.1 mV/dec, respectively. The SPS pellet demonstrates a superior HER activity with the lowest Tafel slope (97.3 mV/dec), indicating a much more efficient HER with faster kinetics versus the other two electrodes. Additionally, the Tafel slope values of the bulk powder and the sonicated powder near 120 mV/dec indicate that the Volmer reaction strongly controls the HER process,[50,51] whereas the SPS pellet shows the Tafel slope falling in between the Volmer reaction (Tafel slope ∼120 mV/dec) and the Heyrovsky reaction (Tafel slope ∼40 mV/dec) due to the complexity of the reaction observed in highly active bulk catalysts.[46] Continuous cyclic voltammetry (CV) was employed to evaluate the stability of FGT (Figure S9a, c, and e). All the electrodes reveal good stability after 3000 cycles. Furthermore, the catalysts were analyzed through a chronoamperometric test (Figure S9b, d, and f). At a fixed overpotential, all the

https://dx.doi.org/10.1021/acsmaterialslett.1c00048
ACS Materials Lett. 2021, 3, 313−319

electrodes yielded a stable current density of about 10 mA/cm^2 for 24 h, further consolidating their high durability.

First-principles DFT calculations were performed to study the active sites of FGT by considering different H-adsorption sites on two different layers, the basal plane (002) and an edge plane (106). For the (002) all tellurium layer, the following sites were considered: (1) on top (Top) of a Te atom, (2) on a hollow site (Hol-1) above an Fe atom, and (3) on a hollow site (Hol-2) above a Ge atom (Figure 4b). For the mixed tellurium/iron (106) layer, the following sites were considered: (4) on top (Top-1) of one Fe atom, (5) on top of a separate Fe atom (Top-2), and (6) on top of a Te atom (Top-3) (Figure 4c). The binding energy (ΔE_H) and the Gibbs free energy (ΔG_H) for H-adsorption were evaluated (see the Supporting Information for more details) for all these sites and compared with those reported for 1T′-$MoTe_2$. As shown in Figure 4a, the calculated ΔG_H values for the basal (002) layer of FGT are 1.30, 1.38, and 1.98 eV for the Top, Hol-1, and Ho1-2 sites, respectively, while for the (106) layer, the obtained ΔG_H values are −0.45, −0.26, and 0.21 eV for the Top-1, Top-2, and Top-3 sites, respectively. Bulk $MoTe_2$ is known for high basal plane activity in its monoclinic polymorph 1T′-$MoTe_2$,[43,52] thus it is the perfect candidate for comparison. The basal plane of this material also contains many active sites on its distorted tellurium layer, two of which have the best ΔG_H values: 0.86 and 1.72 eV for H-adsorption on top of the lower Te and on top of the higher Te, respectively.[52] Comparing the basal plane results of the two phases, it is quite astonishing that the top sites (most active sites for the FGT basal plane) in both compounds have almost the exact ΔG_H values if the average (1.29 eV) is used in the case of 1T′-$MoTe_2$, thus predicting similar HER activity for the basal plane in these two compounds. Indeed, the experimental HER activity measurements presented above for bulk FGT show nearly the same overpotential (η_{10} = −0.337 V, in KOH) as bulk 1T′-$MoTe_2$ (η_{10} = −0.34 V, in H_2SO_4). To the best of our knowledge, FGT is the first HER electrocatalyst found so far in the class of hexagonal vdW materials with an active undistorted hexagonal Te layer, since the hexagonal polymorph of $MoTe_2$ was found not to be competitive for HER in the bulk (Table S3). Furthermore, the results for the (106) layer suggest the presence of an even more active layer for FGT with ΔG_H values that are much closer to zero (from −0.45 to 0.21 eV) in comparison to those calculated for the basal planes of FGT and 1T′-$MoTe_2$. This result supports the far better HER activity found for the sonicated sample if compared to the bulk because smaller particles expose more edge sites which are more active. However, the XPS results showed that a thin oxide layer is present on the surface of these materials, suggesting that the real active sites may be hybrid layers composed of the thin oxide layer and the different active FGT layers underneath. The hybrid model is supported by the fact that a further oxidation (see Figure S11) of the FGT sample through ball-milling has resulted in a significantly bad catalyst despite obvious reduction of particle size according to PXRD.

In conclusion, FGT has been successfully synthesized by a solid-state reaction, and the sample was characterized by PXRD, EDS, and SEM analyses. In addition, its electrochemical properties were studied experimentally and theoretically. Three types of electrodes (bulk powder, sonicated powder, and SPS-densified pellet) were prepared to explore the HER activity. The results indicated that the HER activity of the sonicated FGT, which exposes more basal and edge planes, is higher than that of the bulk. Moreover, the SPS pellet electrode, which is the densest and whose PXRD showed not only single-crystal-like preferred orientation along the *c*-direction but also the presence of some edge planes, requires the smallest overpotential (η_{10} = −0.105 V) among all bulk TMDs reported so far. All the electrodes have excellent long-term stability and durability, displaying no significant HER activity loss after 3000 cycles and 24 h of operation in an alkaline electrolyte. To understand the excellent HER activity of FGT, DFT calculations were performed. The calculated ΔG_H values of the hexagonal basal plane Te layer were found to be nearly equal to that of the puckered Te layer in monoclinic $MoTe_2$ (1T′-$MoTe_2$), supporting the basal plane activity of FGT. Furthermore, the calculated ΔG_H values of another prevalent (106) layer (edge layer) are even closer to zero, thus supporting the increase in activity with particle size reduction, which favors increased edge sites. Furthermore, the presence of a thin oxide layer on top of the active FGT layers as found by XPS suggests that the real active surface is likely a hybrid FGT/oxide layer. This study introduces FGT as a highly HER active hexagonal vdW material with active basal plane and edge sites, thus paving the way for further studies of related iron-based vdW materials, their composites, and their surface functionalization as high-performing electrocatalysts.

■ ASSOCIATED CONTENT

Supporting Information

The Supporting Information is available free of charge at https://pubs.acs.org/doi/10.1021/acsmaterialslett.1c00048.

Chemicals and synthesis procedure, structural characterization, electrode preparation method, electrochemical characterization, density functional theory computations, additional graphs, and tables (PDF)

■ AUTHOR INFORMATION

Corresponding Author

Boniface P. T. Fokwa − *Materials Science and Engineering and Department of Chemistry and Center for Catalysis, University of California, Riverside, California 92521, United States*; orcid.org/0000-0001-9802-7815; Email: bfokwa@ucr.edu; https://fokwalab.ucr.edu/

Authors

Amir A. Rezaie − *Materials Science and Engineering, University of California, Riverside, California 92521, United States*

Eunsoo Lee − *Department of Chemical and Environmental Engineering, University of California, Riverside, California 92521, United States*

Diana Luong − *Department of Chemistry and Center for Catalysis, University of California, Riverside, California 92521, United States*

Johan A. Yapo − *Department of Chemistry and Center for Catalysis, University of California, Riverside, California 92521, United States*

Complete contact information is available at: https://pubs.acs.org/10.1021/acsmaterialslett.1c00048

Author Contributions

#A.A.R., E.L., and D.L. are co-first authors.

Notes

The authors declare no competing financial interest.

https://dx.doi.org/10.1021/acsmaterialslett.1c00048
ACS Materials Lett. 2021, 3, 313−319

■ ACKNOWLEDGMENTS

This work was supported by the startup fund to B.P.T.F. at UC Riverside and partial support from the National Science Foundation Career award to B.P.T.F. (no. DMR-1654780). The authors would like to thank Suveen N. Mathaudhu and Steven Herzberg for their advice and access to the SPS machine. The San Diego Supercomputer Center (SDSC) is gratefully acknowledged for providing computing resources. The XPS data were collected with an instrument acquired through the NSF MRI program (DMR-0958796).

■ REFERENCES

(1) Chow, J.; Kopp, R. J.; Portney, P. R. Energy resources and global development. *Science* **2003**, *302*, 1528−1531.
(2) Roger, I.; Shipman, M. A.; Symes, M. D. Earth-abundant catalysts for electrochemical and photoelectrochemical water splitting. *Nature Reviews Chemistry* **2017**, *1*, 0003.
(3) Turner, J. A. Sustainable hydrogen production. *Science* **2004**, *305*, 972−974.
(4) Bonaccorso, F.; Colombo, L.; Yu, G.; Stoller, M.; Tozzini, V.; Ferrari, A. C.; Ruoff, R. S.; Pellegrini, V. Graphene, related two-dimensional crystals, and hybrid systems for energy conversion and storage. *Science* **2015**, *347*, 1246501.
(5) Xie, Z.; He, P.; Du, L.; Dong, F.; Dai, K.; Zhang, T. Comparison of four nickel-based electrodes for hydrogen evolution reaction. *Electrochim. Acta* **2013**, *88*, 390−394.
(6) McCrory, C. C.; Jung, S.; Ferrer, I. M.; Chatman, S. M.; Peters, J. C.; Jaramillo, T. F. Benchmarking hydrogen evolving reaction and oxygen evolving reaction electrocatalysts for solar water splitting devices. *J. Am. Chem. Soc.* **2015**, *137*, 4347−4357.
(7) Lewis, N. S.; Nocera, D. G. Powering the planet: Chemical challenges in solar energy utilization. *Proc. Natl. Acad. Sci. U. S. A.* **2006**, *103*, 15729−15735.
(8) Cook, T. R.; Dogutan, D. K.; Reece, S. Y.; Surendranath, Y.; Teets, T. S.; Nocera, D. G. Solar energy supply and storage for the legacy and nonlegacy worlds. *Chem. Rev.* **2010**, *110*, 6474−6502.
(9) Park, S.; Shao, Y.; Liu, J.; Wang, Y. Oxygen electrocatalysts for water electrolyzers and reversible fuel cells: status and perspective. *Energy Environ. Sci.* **2012**, *5*, 9331−9344.
(10) Feng, J.; Lv, F.; Zhang, W.; Li, P.; Wang, K.; Yang, C.; Wang, B.; Yang, Y.; Zhou, J.; Lin, F. Iridium-based multimetallic porous hollow nanocrystals for efficient overall-water-splitting catalysis. *Adv. Mater.* **2017**, *29*, 1703798.
(11) Dillon, J., Jr; Kamimura, H.; Remeika, J. Magneto-optical properties of ferromagnetic chromium trihalides. *J. Phys. Chem. Solids* **1966**, *27*, 1531−1549.
(12) Neto, A. H. C.; Guinea, F.; Peres, N. M.; Novoselov, K. S.; Geim, A. K. The electronic properties of graphene. *Rev. Mod. Phys.* **2009**, *81*, 109.
(13) Novoselov, K. S.; Geim, A. K.; Morozov, S. V.; Jiang, D.; Zhang, Y.; Dubonos, S. V.; Grigorieva, I. V.; Firsov, A. A. Electric field effect in atomically thin carbon films. *Science* **2004**, *306*, 666−669.
(14) Mas-Balleste, R.; Gomez-Navarro, C.; Gomez-Herrero, J.; Zamora, F. 2D materials: to graphene and beyond. *Nanoscale* **2011**, *3*, 20−30.
(15) Mak, K. F.; Shan, J. Photonics and optoelectronics of 2D semiconductor transition metal dichalcogenides. *Nat. Photonics* **2016**, *10*, 216.
(16) Pomerantseva, E.; Gogotsi, Y. Two-dimensional heterostructures for energy storage. *Nature Energy* **2017**, *2*, 17089.
(17) Li, H.; Tsai, C.; Koh, A. L.; Cai, L.; Contryman, A. W.; Fragapane, A. H.; Zhao, J.; Han, H. S.; Manoharan, H. C.; Abild-Pedersen, F. Activating and optimizing MoS 2 basal planes for hydrogen evolution through the formation of strained sulphur vacancies. *Nat. Mater.* **2016**, *15*, 48−53.
(18) Voiry, D.; Fullon, R.; Yang, J.; e Silva, C. d. C. C.; Kappera, R.; Bozkurt, I.; Kaplan, D.; Lagos, M. J.; Batson, P. E.; Gupta, G. The role of electronic coupling between substrate and 2D MoS 2 nanosheets in electrocatalytic production of hydrogen. *Nat. Mater.* **2016**, *15*, 1003−1009.
(19) Wang, Y.; Li, Y.; Heine, T. PtTe Monolayer: Two-Dimensional Electrocatalyst with High Basal Plane Activity toward Oxygen Reduction Reaction. *J. Am. Chem. Soc.* **2018**, *140*, 12732−12735.
(20) Zhao, Y.; Gu, J.; Chen, Z. Oxygen Evolution Reaction on 2D Ferromagnetic Fe3GeTe2: Boosting the Reactivity by the Self-Reduction of Surface Hydroxyl. *Adv. Funct. Mater.* **2019**, *29*, 1904782.
(21) Li, D.; Jia, Y.; Chang, G.; Chen, J.; Liu, H.; Wang, J.; Hu, Y.; Xia, Y.; Yang, D.; Yao, X. A defect-driven metal-free electrocatalyst for oxygen reduction in acidic electrolyte. *Chem.* **2018**, *4*, 2345−2356.
(22) Li, Y.; Yin, K.; Wang, L.; Lu, X.; Zhang, Y.; Liu, Y.; Yan, D.; Song, Y.; Luo, S. Engineering MoS2 nanomesh with holes and lattice defects for highly active hydrogen evolution reaction. *Appl. Catal., B* **2018**, *239*, 537−544.
(23) Ou, G.; Fan, P.; Ke, X.; Xu, Y.; Huang, K.; Wei, H.; Yu, W.; Zhang, H.; Zhong, M.; Wu, H. Defective molybdenum sulfide quantum dots as highly active hydrogen evolution electrocatalysts. *Nano Res.* **2018**, *11*, 751−761.
(24) Zhu, Z.; Yin, H.; He, C. T.; Al-Mamun, M.; Liu, P.; Jiang, L.; Zhao, Y.; Wang, Y.; Yang, H. G.; Tang, Z. Ultrathin transition metal dichalcogenide/3d metal hydroxide hybridized nanosheets to enhance hydrogen evolution activity. *Adv. Mater.* **2018**, *30*, 1801171.
(25) Gao, M.-R.; Liang, J.-X.; Zheng, Y.-R.; Xu, Y.-F.; Jiang, J.; Gao, Q.; Li, J.; Yu, S.-H. An efficient molybdenum disulfide/cobalt diselenide hybrid catalyst for electrochemical hydrogen generation. *Nat. Commun.* **2015**, *6*, 5982.
(26) Hong, H.; Liu, C.; Cao, T.; Jin, C.; Wang, S.; Wang, F.; Liu, K. Interfacial engineering of van der waals coupled 2D layered materials. *Adv. Mater. Interfaces* **2017**, *4*, 1601054.
(27) Qin, Y.; Wu, H.-H.; Zhang, L. A.; Zhou, X.; Bu, Y.; Zhang, W.; Chu, F.; Li, Y.; Kong, Y.; Zhang, Q. Aluminum and nitrogen codoped graphene: Highly active and durable electrocatalyst for oxygen reduction reaction. *ACS Catal.* **2019**, *9*, 610−619.
(28) Luo, Z.; Ouyang, Y.; Zhang, H.; Xiao, M.; Ge, J.; Jiang, Z.; Wang, J.; Tang, D.; Cao, X.; Liu, C. Chemically activating MoS 2 via spontaneous atomic palladium interfacial doping towards efficient hydrogen evolution. *Nat. Commun.* **2018**, *9*, 2120.
(29) Zhao, Y.; Wan, J.; Yao, H.; Zhang, L.; Lin, K.; Wang, L.; Yang, N.; Liu, D.; Song, L.; Zhu, J. Few-layer graphdiyne doped with sp-hybridized nitrogen atoms at acetylenic sites for oxygen reduction electrocatalysis. *Nat. Chem.* **2018**, *10*, 924−931.
(30) Abrikosov, N. K.; Bagaeva, L.; Dudkin, L. Phase equilibria in Fe-Ge-Te system. *Izv. Akad. Nauk SSSR, Neorg. Mater.* **1985**, *21*, 1680−1686.
(31) Deiseroth, H. J.; Aleksandrov, K.; Reiner, C.; Kienle, L.; Kremer, R. K. Fe3GeTe2 and Ni3GeTe2−Two New Layered Transition-Metal Compounds: Crystal Structures, HRTEM Investigations, and Magnetic and Electrical Properties. *Eur. J. Inorg. Chem.* **2006**, *2006*, 1561−1567.
(32) Cui, Z.; Xiao, C.; Lv, Y.; Li, Q.; Sa, R.; Ma, Z. Adsorption behavior of CO, CO2, H2, H2O, NO, and O2 on pristine and defective 2D monolayer Ferromagnetic Fe3GeTe2. *Appl. Surf. Sci.* **2020**, *527*, 146894.
(33) Yan, Y.; Xia, B. Y.; Ge, X.; Liu, Z.; Fisher, A.; Wang, X. A flexible electrode based on iron phosphide nanotubes for overall water splitting. *Chem. - Eur. J.* **2015**, *21*, 18062−18067.
(34) Grosvenor, A. P.; Wik, S. D.; Cavell, R. G.; Mar, A. Examination of the bonding in binary transition-metal monophosphides MP (M= Cr, Mn, Fe, Co) by X-ray photoelectron spectroscopy. *Inorg. Chem.* **2005**, *44*, 8988−8998.
(35) Li, H.; Wen, P.; Li, Q.; Dun, C.; Xing, J.; Lu, C.; Adhikari, S.; Jiang, L.; Carroll, D. L.; Geyer, S. M. Earth-abundant iron diboride (FeB2) nanoparticles as highly active bifunctional electrocatalysts for overall water splitting. *Adv. Energy Mater.* **2017**, *7*, 1700513.
(36) Liang, R.; Shen, L.; Jing, F.; Qin, N.; Wu, L. Preparation of MIL-53 (Fe)-reduced graphene oxide nanocomposites by a simple self-assembly strategy for increasing interfacial contact: efficient

https://dx.doi.org/10.1021/acsmaterialslett.1c00048
ACS Materials Lett. 2021, 3, 313−319

visible-light photocatalysts. *ACS Appl. Mater. Interfaces* **2015**, *7*, 9507−9515.
(37) Grossi, V.; Ottaviano, L.; Santucci, S.; Passacantando, M. XPS and SEM studies of oxide reduction of germanium nanowires. *J. Non-Cryst. Solids* **2010**, *356*, 1988−1993.
(38) Huang, Y.; Xu, J.-P.; Liu, L.; Lai, P.-T.; Tang, W.-M. N 2-Plasma-Treated Ga 2 O 3 (Gd 2 O 3) as Interface Passivation Layer for Ge MOS Capacitor With HfTiON Gate Dielectric. *IEEE Trans. Electron Devices* **2016**, *63*, 2838−2843.
(39) Xie, Q.; Deng, S.; Schaekers, M.; Lin, D.; Caymax, M.; Delabie, A.; Qu, X.-P.; Jiang, Y.-L.; Deduytsche, D.; Detavernier, C. Germanium surface passivation and atomic layer deposition of high-k dielectrics—A tutorial review on Ge-based MOS capacitors. *Semicond. Sci. Technol.* **2012**, *27*, 074012.
(40) Yang, Z.; Xu, M.; Cheng, X.; Tong, H.; Miao, X. Manipulation of dangling bonds of interfacial states coupled in GeTe-rich GeTe/Sb 2 Te 3 superlattices. *Sci. Rep.* **2017**, *7*, 17353.
(41) Reese, M. O.; Perkins, C. L.; Burst, J. M.; Farrell, S.; Barnes, T. M.; Johnston, S. W.; Kuciauskas, D.; Gessert, T. A.; Metzger, W. K. Intrinsic surface passivation of CdTe. *J. Appl. Phys.* **2015**, *118*, 155305.
(42) Toh, R. J.; Sofer, Z.; Luxa, J.; Sedmidubský, D.; Pumera, M. 3R phase of MoS 2 and WS 2 outperforms the corresponding 2H phase for hydrogen evolution. *Chem. Commun.* **2017**, *53*, 3054−3057.
(43) McGlynn, J. C.; Cascallana-Matías, I.; Fraser, J. P.; Roger, I.; McAllister, J.; Miras, H. N.; Symes, M. D.; Ganin, A. Y. Molybdenum ditelluride rendered into an efficient and stable electrocatalyst for the hydrogen evolution reaction by polymorphic control. *Energy Technology* **2018**, *6*, 345−350.
(44) Trasatti, S.; Petrii, O. Real surface area measurements in electrochemistry. *Pure Appl. Chem.* **1991**, *63*, 711−734.
(45) McGlynn, J. C.; Dankwort, T.; Kienle, L.; Bandeira, N. A.; Fraser, J. P.; Gibson, E. K.; Cascallana-Matías, I.; Kamarás, K.; Symes, M. D.; Miras, H. N.; Ganin, A.Y. The rapid electrochemical activation of MoTe 2 for the hydrogen evolution reaction. *Nat. Commun.* **2019**, *10*, 4916.
(46) Park, H.; Zhang, Y.; Lee, E.; Shankhari, P.; Fokwa, B. P. High-Current-Density HER Electrocatalysts: Graphene-like Boron Layer and Tungsten as Key Ingredients in Metal Diborides. *ChemSusChem* **2019**, *12*, 3726−3731.
(47) Park, H.; Lee, E.; Lei, M.; Joo, H.; Coh, S.; Fokwa, B. P. Canonic-Like HER Activity of Cr1−xMoxB2 Solid Solution: Overpowering Pt/C at High Current Density. *Adv. Mater.* **2020**, *32*, 2000855.
(48) Lee, E.; Park, H.; Joo, H.; Fokwa, B. P. Unexpected Correlation Between Boron Chain Condensation and Hydrogen Evolution Reaction (HER) Activity in Highly Active Vanadium Borides: Enabling Predictions. *Angew. Chem., Int. Ed.* **2020**, *59*, 11774−11778.
(49) Zhou, W.; Chen, M.; Guo, M.; Hong, A.; Yu, T.; Luo, X.; Yuan, C.; Lei, W.; Wang, S. Magnetic enhancement for hydrogen evolution reaction on ferromagnetic MoS2 catalyst. *Nano Lett.* **2020**, *20*, 2923−2930.
(50) Chung, D. Y.; Park, S.-K.; Chung, Y.-H.; Yu, S.-H.; Lim, D.-H.; Jung, N.; Ham, H. C.; Park, H.-Y.; Piao, Y.; Yoo, S. J. Edge-exposed MoS 2 nano-assembled structures as efficient electrocatalysts for hydrogen evolution reaction. *Nanoscale* **2014**, *6*, 2131−2136.
(51) Sheng, W.; Gasteiger, H. A.; Shao-Horn, Y. Hydrogen oxidation and evolution reaction kinetics on platinum: acid vs alkaline electrolytes. *J. Electrochem. Soc.* **2010**, *157*, B1529−B1536.
(52) You, H.; Zhuo, Z.; Lu, X.; Liu, Y.; Guo, Y.; Wang, W.; Yang, H.; Wu, X.; Li, H.; Zhai, T. 1T′-MoTe2-Based On-Chip Electrocatalytic Microdevice: A Platform to Unravel Oxidation-Dependent Electrocatalysis. *CCS Chemistry* **2019**, *1*, 396−406.

https://dx.doi.org/10.1021/acsmaterialslett.1c00048
ACS Materials Lett. 2021, 3, 313−319